International Journal of Nanomedicine

Dovepress
open access to scientific and medical research

Open Access Full Text Article

ORIGINAL RESEARCH

Synthesis and characterization of silver/talc nanocomposites using the wet chemical reduction method

This article was published in the following Dove Press journal:
International Journal of Nanomedicine
28 September 2010
Number of times this article has been viewed

Kamyar Shameli[1]
Mansor Bin Ahmad[1]
Wan Zin Wan Yunus[1]
Nor Azowa Ibrahim[1]
Majid Darroudi[2]

[1]Department of Chemistry, Faculty of Science, [2]Advanced Materials and Nanotechnology Laboratory, Institute of Advanced Technology, Universiti Putra Malaysia, Selangor, Malaysia

Abstract: In this study, silver nanoparticles (Ag-NPs) were synthesized using the wet chemical reduction method on the external surface layer of talc mineral as a solid support. Silver nitrate and sodium borohydride were used as the silver precursor and reducing agent in talc. The talc was suspended in aqueous $AgNO_3$ solution. After the absorption of Ag^+ on the surface, the ions were reduced with $NaBH_4$. The interlamellar space limits were without many changes (d_s = 9.34–9.19 A°); therefore, Ag-NPs formed on the exterior surface of talc, with d_{ave} = 7.60–13.11 nm in diameter. The properties of Ag/talc nanocomposites (Ag/talc-NCs) and the diameters of the Ag-NPs prepared in this way depended on the primary $AgNO_3$ concentration. The prepared Ag-NPs were characterized by ultraviolet-visible spectroscopy, powder X-ray diffraction, transmission electron microscopy, scanning electron microscopy, and Fourier transform infrared. These Ag/talc-NCs may have potential applications in the chemical and biological industries.

Keywords: nanocomposites, silver nanoparticles, talc, powder X-ray diffraction, scanning electron microscopy

Introduction

Metal nanoparticles, which consist of novel metals, have significant applications in medical identification, catalysis, sensors, optics, and electronics, because of the characteristics of their shapes and sizes.[1–6] When metal nanoparticles are used alone, they present some common problems, particularly agglomeration between nanoparticles.[7] To overcome agglomeration, preparation of nanoparticles based on clay compounds, in which nanoparticles are supported within the interlamellar spaces of clay and/or on the external surfaces, is one of the most effective solutions.[8–10] Synthesis of nanoparticle/clay composites is very important in the fabrication of such different tools as optical devices, adsorbents, catalysts, sensors, polarizers, color filters, magnetic data storage media, and many others.[11–18] The main characteristics of these nanocomposites are the size and shape of the incorporated metal nanoparticles, as well as the chemical and physical properties of the clay source (ie, ion absorption capacity, active surface area, and interlamellar space). Different techniques can be used to achieve metal/clay nanocomposites, ie, distribution of nanoparticles from chemically produced metal nanoparticles in the clay matrix and by synthesis of metal nanoparticles outside and inside the clay matrix using physical methods. In addition, the wet chemical reduction method can be used for immobilization of noble metal nanoparticles on the external and interior surfaces of silicate layers.[19]

Correspondence: Kamyar Shameli
Department of Chemistry, Faculty of Science, Universiti Putra Malaysia, 43400 UPM Serdang, Selangor, Malaysia
Tel +60 389 466 793
Fax +60 389 435 380
Email kamyarshameli@gmail.com

Silver nanoparticles (Ag-NPs) are a typical metal of nanomaterials, and the synthesis of silver/clay nanocomposites has been discussed in a number of publications.[20–22] Notably, silver nanoparticles are widely used as antibacterial agents,[23,24] catalysts, photocatalysts,[25,26] photosensitive components,[27] and the surface enhancer for Raman spectroscopy.[28,29] Talc is a nonexpandable lamellar hydrated form of magnesium silicate, with the empiric formula of $Mg_3Si_4O_{10}(OH)_2$. It is used as a filler material for polymer and rubber, and is utilized extensively in cosmetic and pharmaceutical powders. The talc surface is extremely hydrophobic and, thus, in a finely ground state, will actually float on the surface of water. This natural phyllosilicate is formed over millions of years by the alteration of certain minerals, such as magnesite ($MgCO_3$) or dolomite [$MgCa(CO_3)_2$], under heat and pressure changes and in the presence of dissolved silica. Due to variation in the physical conditions during this process, all talcs diverge in some features in their composition, because the formation conditions differ from their distinct origins.[30,31] The natural lamellar talc structure consists of layers 0.96 nm thick constructed from a central sheet of octahedrally coordinated magnesium hydroxide in a trioctahedral arrangement sandwiched between tetrahedrally coordinated Si_2O_5 silicate sheets.[32] The crystal arrangement of talc is reflected in physical properties, including its excellent cleavage in the direction of the plane of silicon oxide anions. This is due to weak van der Waals bonds between the packets. The softness of talc is also due to the easy displacement of these layers, rendering the material a poor electrical and thermal, refractory behavior, and resistant to acids. The attractive forces between the sheets give the matrix a nonexpandable characteristic and, consequently, the chemical reactivity is limited to modifications on the surface.[33]

In this research, Ag-NPs were synthesized on the external surface of talc layers in aqueous solution using $AgNO_3$ and sodium borohydride as the silver precursor and reduction agent, respectively, at room temperature. Needless to say, to date, there has not been any research on Ag/talc nanocomposites (Ag/talc-NCs) using the wet chemical reducing method, ie, lamellar polymeric silicate, which is the subject of this study.

Material and methods

Material

All reagents in this work were of analytical grade and used as received without further purification. $AgNO_3$ of 99.98% was used as the silver precursor and obtained from Merck, Germany, while the talc powder of <10 microns and $NaBH_4$ of 98.5% were obtained from Sigma-Aldrich, St Louis, MO. All these aqueous solutions were used with double distilled water.

Synthesis of Ag/talc-NCs using $NaBH_4$

For the synthesis of Ag/talc-NCs, the silver contents of the samples consisted of 0.5 (A1), 1.0 (A2), 1.5 (A3), 2.0 (A4), and 5.0 g (A5) Ag/100 g of talc. Constant amounts of talc were suspended in different volumes of 1×10^{-3} M $AgNO_3$ solution and stirred for 24 hours. The freshly prepared $NaBH_4$ (4×10^{-2} M) solution was then added to the suspensions under continuous stirring to reach a constant $AgNO_3/NaBH_4$ molar ratio of 1:4. After addition of the reducing agent, stirring was continued for a further hour. The suspensions were finally centrifuged, washed twice with double distilled water, and dried under vacuum overnight. All the experiments were conducted at ambient temperature.

Characterization methods and instruments

The prepared Ag/talc-NCs were characterized by ultraviolet (UV)-visible spectroscopy, transmission electron microscopy (TEM), scanning electron microscopy (SEM), powder X-ray diffraction (PXRD), and Fourier transform infrared (FT-IR). The UV-visible spectra were recorded over the range of 300–700 nm using a Lambda 25-PerkinElmer UV-visible spectrophotometer. Meanwhile, the TEM observations were carried out using an Hitachi H-7100 electron microscope, and the particle size distributions were determined using the UTHSCSA Image Tool software, version 3.00 program. Furthermore, SEM was performed utilizing the XL 30 Philips instrument to study the morphology of talc and Ag/talc-NCs. The structures of the Ag/talc-NCs produced were

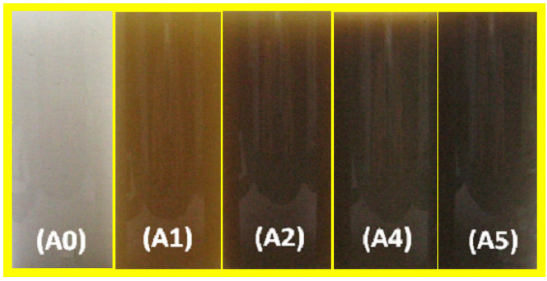

Figure 1 Photographs of $AgNO_3$/talc suspension (A0) and silver-talc nanocomposite suspension at different $AgNO_3$ concentrations, ie, (A1) 0.5%, (A2) 1.0%, (A4) 2.0%, and (A5) 5%.

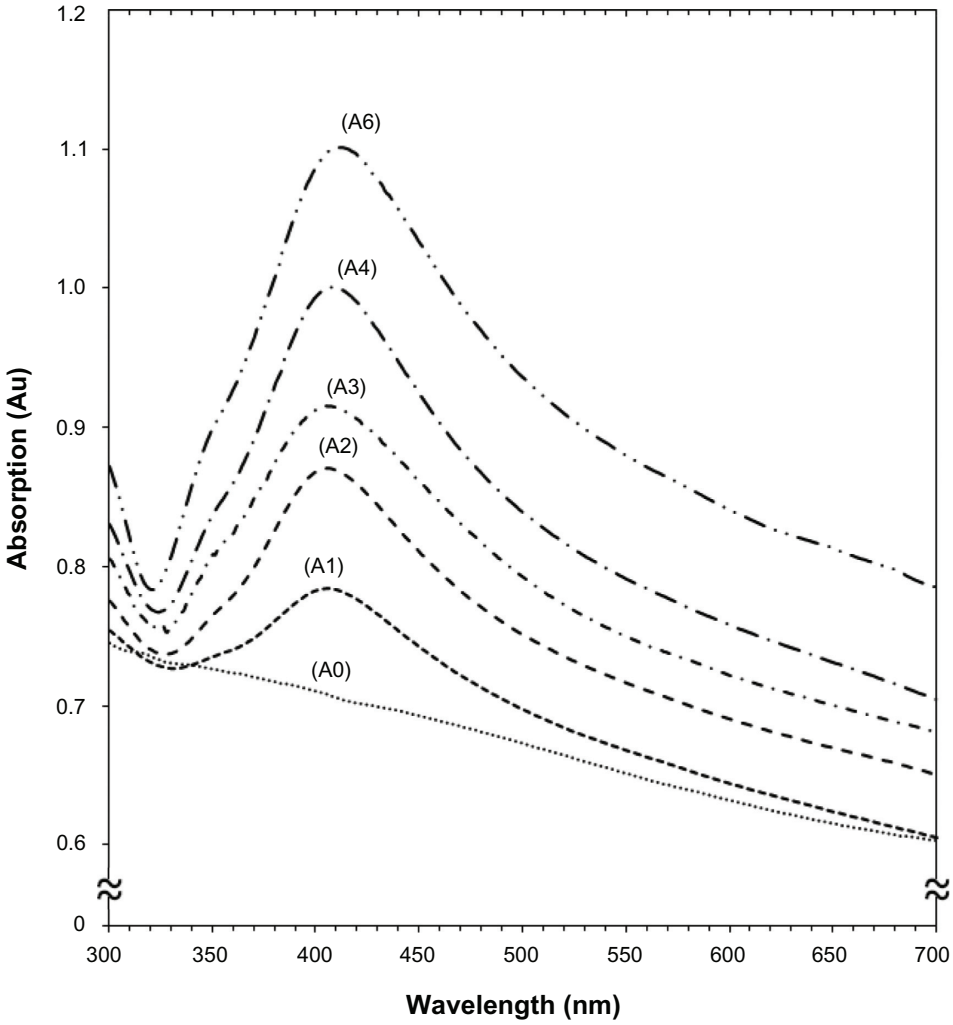

Figure 2 Ultraviolet-visible absorption spectra of silver-talc nanocomposite suspensions for different $AgNO_3$ concentrations, ie, (A1) 0.5%, (A2) 1.0%, (A3) 1.5%, (A4) 2.0%, (A5) 5%, and (A0) $AgNO_3$/talc suspension in the absence of $NaBH_4$.

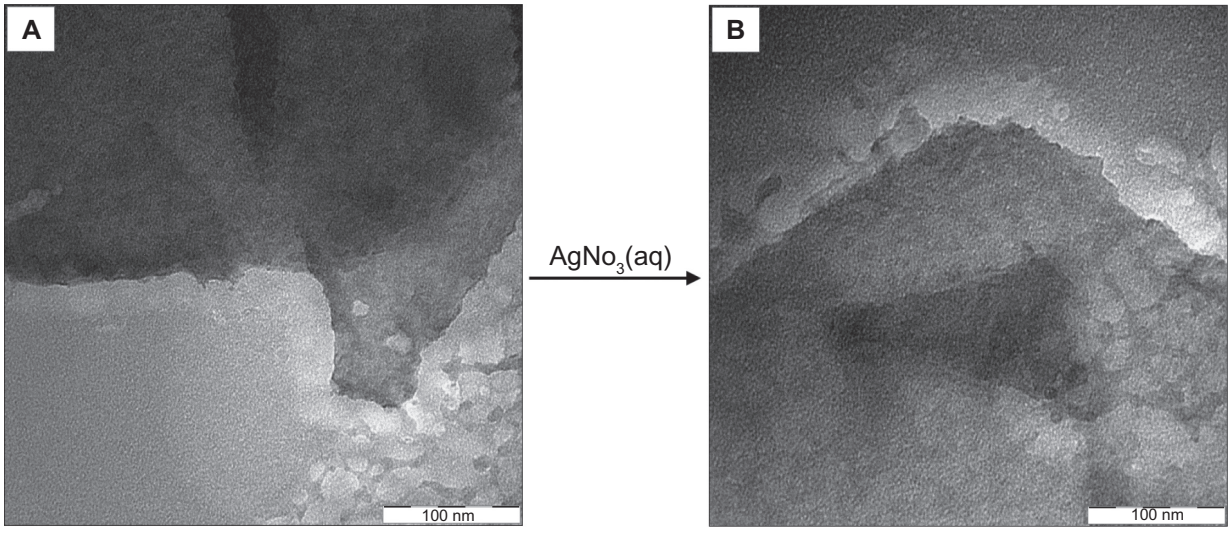

Figure 3 Transmission electron microscopy images of (**A**) pure talc and (**B**) talc after impregnation with aqueous $AgNO_3$ ($AgNO_3$/talc, A0).

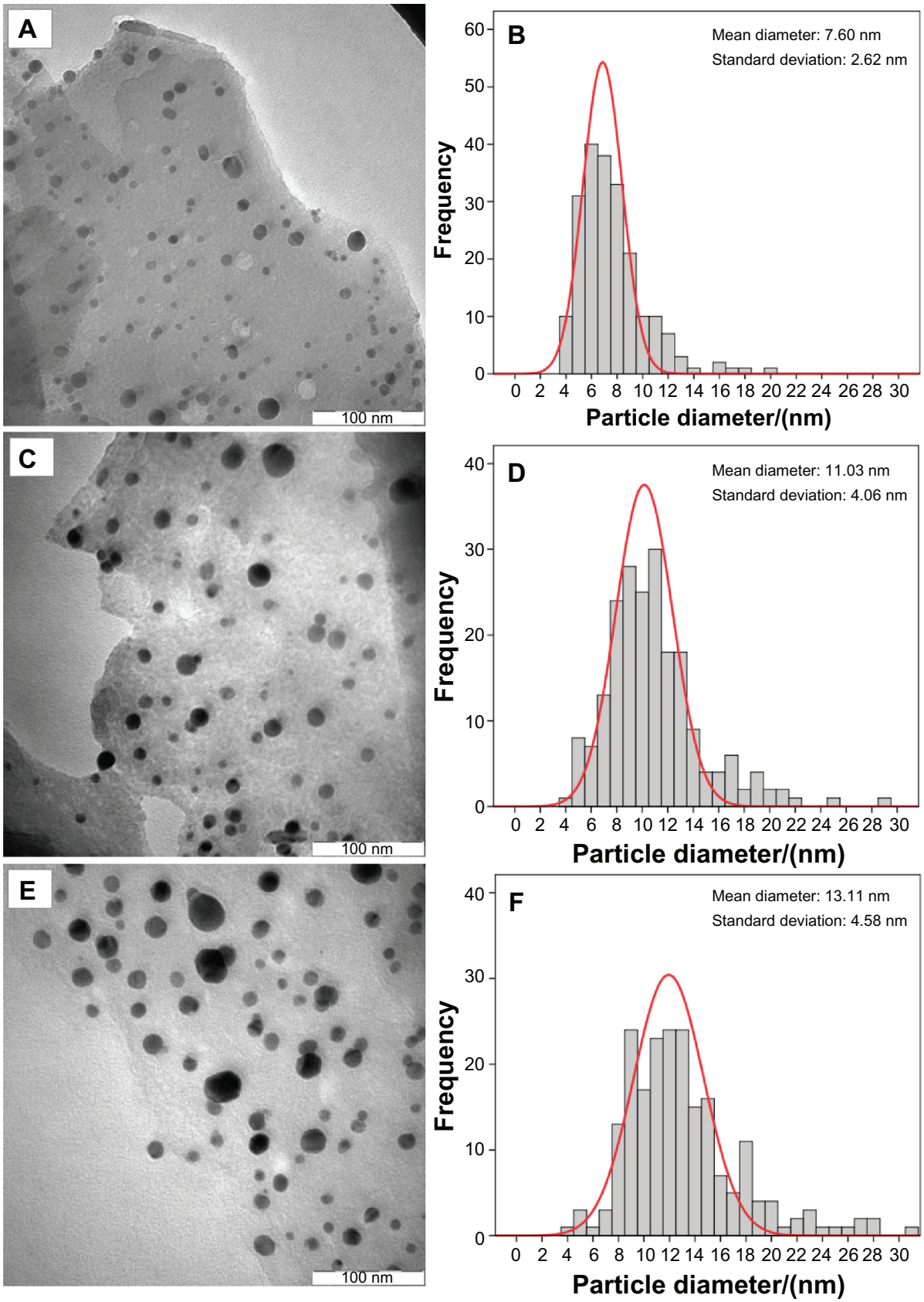

Figure 4 Transmission electron microscopy images and corresponding particle size distribution of silver-talc nanocomposites at different $AgNO_3$ concentrations [(A2) 1.0% (**A–B**), (A4) 2.0% (**C–D**) and (A5) 5.0% (**E–F**)].

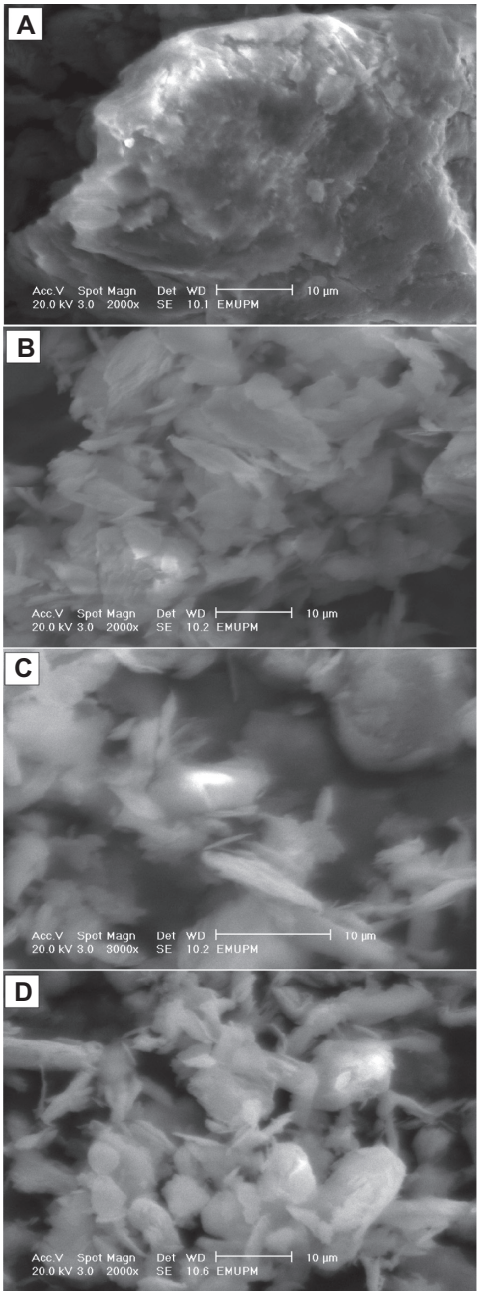

Figure 5 Scanning electron microscopy micrographs of the talc (**A**) and silver-talc nanocomposites at different $AgNO_3$ concentrations [(A2) 1.0% (**B**), (A4) 2.0% (**C**), and (A5) 5.0% (**D**)].

examined using Philips PXRD (X'pert, Cu K_α radiation). Changes in the interlamellar spacing of talc and Ag/talc-NCs were also studied using PXRD in the small angle range of $2° < 2\theta < 15°$. In addition, the interlamellar space was calculated based on the PXRD peak positions using Bragg's equation. A wavelength of 0.15418 nm was used for these measurements. The PXRD patterns were recorded at a scan speed of 2° min^{-1}. Moreover, the FT-IR spectra were recorded over the range of 400–4000 cm^{-1} utilizing the Series 100 PerkinElmer FT-IR 1650 spectrophotometer. After the reactions, the samples were centrifuged by using a high-speed centrifuge machine (Avanti J25, Beckman).

Results and discussion

As shown in Figure 1, the $AgNO_3$/talc suspension was colorless (A0), but after the addition of the reducing agent suspensions, it turned to light brown (A1), brown (A2), and dark brown (A4, A5). The formation of Ag-NPs was followed by measuring the surface plasmon resonance of the talc suspensions containing Ag-NPs in the wavelength range 300–700 nm (Figure 2). The TEM images and size distributions of Ag-NPs showed that the mean diameter of the nanoparticles ranged from about 7.60 to 13.11 nm (Figure 4). Additionally, the SEM images indicated that there were no structural changes between the initial talc and Ag/talc-NCs. Meanwhile, with the increased Ag-NP concentration in the talc, the external surface of the talc became shinier (Figure 5). The comparison between the PXRD patterns of talc and the prepared Ag/talc-NCs under the chemical reduction route in the small angle fell in the range of 2θ ($2° < 2\theta < 15°$), which indicated the immobilized formation of Ag-NPs on the external surface of the talc layers (Figure 6). On the other hand, as shown in Figure 7, PXRD patterns were also employed to determine the crystalline structures of synthesized Ag-NPs in the wide angle range of 2θ ($30° < 2\theta < 80°$). Furthermore, FT-IR spectra (Figure 8) showed that there was no interaction between the silicate layers and Ag-NPs in Ag/talc-NCs. The synthesized talc suspensions containing Ag-NPs were found to be unstable over a long period of time, displaying signs of precipitation.

UV-visible spectroscopy

The color of $AgNO_3$/talc suspensions through the reduction process using $NaBH_4$ changed from colorless to light brown, brown, and finally dark brown, which indicated the formation of Ag/talc-NCs suspension. The silver surface plasmon resonance bands were detected at around 404–415 nm (Figure 2). These absorption bands were assumed to correspond to Ag-NPs smaller than 15 nm.[34,35] While there was no UV-visible absorption of Ag-NPs before the addition of $NaBH_4$ in A0 (Figure 1), the growth of the plasmon peak at 404 nm indicates formation of Ag-NPs in A1. Furthermore, the gradual increase in $AgNO_3$ concentration from A1 to A4 also increased the corresponding peak intensities in the

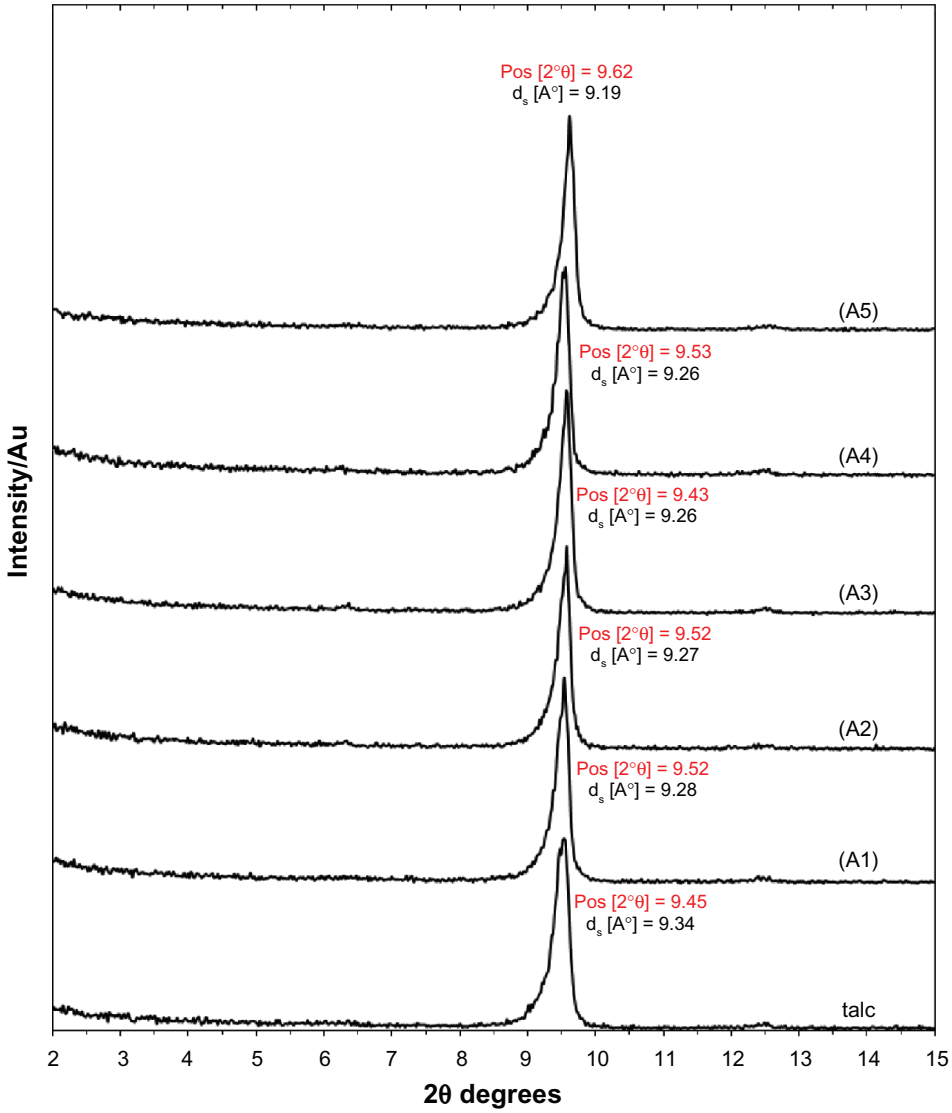

Figure 6 Powder X-ray diffraction patterns of talc and silver-talc nanocomposites for determination of d-spacing (d_s) at different $AgNO_3$ concentrations [0.5%, 1.0%, 1.5%, 2.0% and 5.0% (A1–A5), respectively].

wavelength range 404–411 nm. In A5, the absorption peak due to the surface plasmon resonance of Ag was slightly red-shifted to higher wavelength (415 nm), which indicated an increase in size of the Ag-NPs.

Morphology

Figure 3 illustrates the TEM images of pure talc and talc after impregnation with aqueous $AgNO_3$. Figure 3a demonstrates a typical talc clay image with homogeneously distributed clay flakes, and Figure 3b shows a TEM image for $AgNO_3$/talc (A0), which was similar to the talc image, but without any Ag-NPs. Figure 4 demonstrates TEM images for the size distribution of Ag/talc-NCs containing different percentages of Ag-NPs. The TEM images and their size distributions revealed that the mean diameters and standard deviation of Ag-NPs were about 7.60 ± 2.62, 11.30 ± 4.06, and 13.11 ± 4.58 nm for 1.0% (Figures 4a and 4b), 2.0% (Figures 4c and 4d), and 5.0% (Figures 4e and 4f), respectively. These results demonstrate that the diameters of the Ag-NPs synthesized by this method depend on the initial $AgNO_3$ concentration. Conversely, Figure 5 shows the surface morphology of talc and Ag/talc-NCs (A0, A2, A4, and A5). Furthermore, the structure of talc with or without Ag-NPs showed a massive, layered surface with some large flakes, ie, a typical structure of talc (Figure 5a). More importantly, no morphologic differences were observed between the initial talc and Ag/talc-NCs. Meanwhile, with the increased Ag-NPs concentration in the talc, the external surface of the talc became shinier (Figures 5b–d).

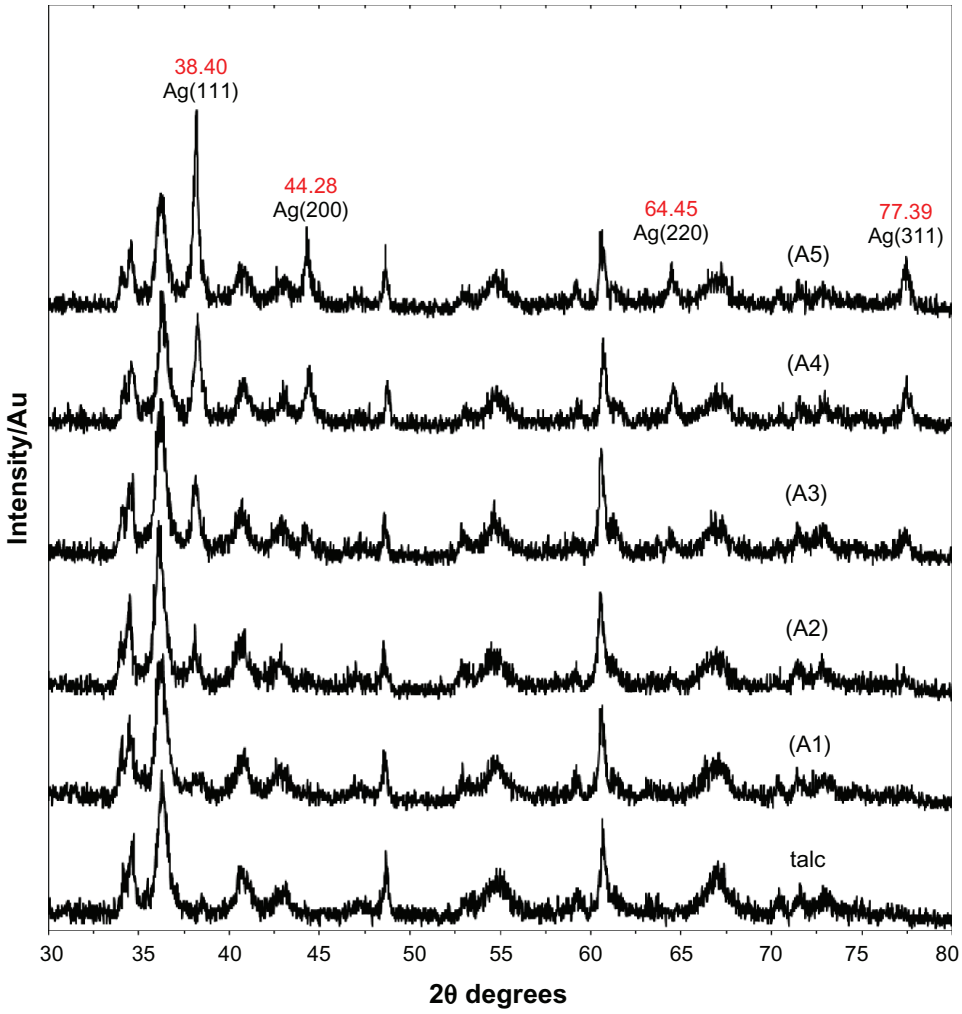

Figure 7 Powder X-ray diffraction patterns of talc and silver-talc nanocomposites for determination of silver crystals at different $AgNO_3$ concentrations [0.5%, 1.0%, 1.5%, 2.0% and 5.0% (A1–A5), respectively].

X-ray diffraction

As shown in Figure 6, the original d-spacing (d_s) of talc, ie, 9.34 A°, gradually decreased to 9.28, 9.27, 9.26, 9.26, and 9.19 A° at constant 2θ angles for A0, A1, A2, A3, A4, and A5 by the Ag-NPs formation on the surface of talc layers. This d_s value was a direct proof of the fact that, in the path of ion impregnation, Ag^+ ions were bound only on the external surfaces and edges of the talc external layer space. Consequently, the metallic nanoparticles formed only at the exterior layer location, causing a decrease in the basal spacing of talc. In all these samples, the intensities of reflections and half-widths were constant; therefore, the parallel lamellar structure of the mineral clay was not disrupted by the formation of nanoparticles.[36] In addition, all the Ag/talc-NCs had a similar diffraction profile, and the PXRD peaks at 2θ of 38.40°, 44.28°, 64.45°, and 77.39° (Figure 7) could be attributed to the 111, 200, 220, and 311 crystallographic planes of the face-centered cubic silver crystals, respectively.[37] For all samples, the main crystalline phase was silver and no obvious other phases as impurities were found in the PXRD patterns. The PXRD peak broadenings of Ag-NPs were mostly due to the existing nanosized particles in these nanocomposites.[38] Moreover, there were characteristic peaks in about 2θ = 34.54°, 36.04°, 40.56°, 42.74°, 48.56°, 54.60°, 60.56°, 66.50°,70.34°, 71.42°, and 72.84° that related to talc (PXRD Reference Number 00–029–1493) as a stable substrate. The intensities of 111, 200, 220, and 311 reflections due to the Ag-NPs phase were also found to increase along with the increased Ag-NPs content.

FT-IR chemical analysis

Figure 8 shows the comparison of FT-IR spectra for the silicate host structure of talc and Ag/talc-NCs with dif-

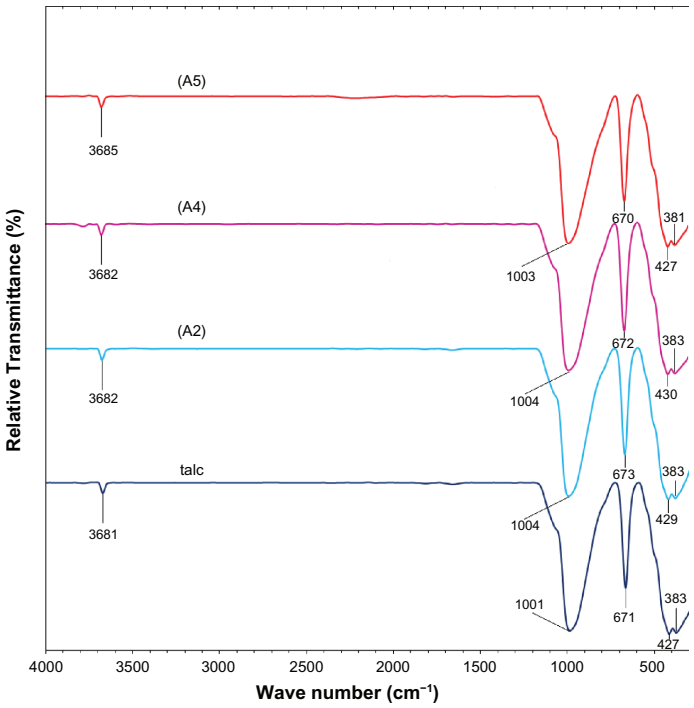

Figure 8 Fourier transform infrared spectra of talc and silver-talc nanocomposites at 1 (A2), 2 (A4) and 5 (A5) wt% silver nanoparticles.

ferent amounts of Ag-NPs. The positions of vibrational bands in the region 1100–400 cm^{-1} corresponding to SiO and other interlayer bonds remained unchanged, and a strong band at 1001 cm^{-1} was associated with the stretching vibration of SiO. The band at 670–673 cm^{-1} was also assigned to the stretching vibration of SiO, which is usually taken as evidence for a three-dimensional amorphous silica phase.[39] The band at 427–383 cm^{-1} was assigned to the Si-O-Si bending vibration. The FT-IR spectra indicated the rigidity of silicate layers and nonbond chemical interaction between the silicate layers and Ag-NPs in Ag/talc-NCs.

Conclusion

The synthesis of Ag-NPs on the exterior layer space of talc as a solid material in the wet chemical reduction method by using $NaBH_4$ as the reducing agent at room temperature was easily feasible. The properties of Ag-NPs were studied as a function of $AgNO_3$ concentration, whereby the molar ratio of $AgNO_3/NaBH_4$ was found to be constant. When the amount of $AgNO_3$ was increased, the particle size of the Ag-NPs gradually increased as well; however, their size distribution was found to be narrow. FT-IR showed that there was no existing chemical interaction between the talc layers and the Ag-NPs.

Acknowledgments

Thanks are due to Mrs Parvaneh Shabanzadeh and Professor Abdolhossein Rustaiyan for their helpful discussion and ideas concerning this study. The authors are also grateful to the Institute of Bioscience at Universiti Putra Malaysia and Mrs Amina Jusoh of the Transmission Electron Microscopy Unit for technical assistance in this project.

Disclosure

The authors have no conflict of interests to disclose in this work.

References

1. Hainfeld JF, Slatkin DN, Focella TM, et al. Gold nanoparticles: A new x-ray contrast agent. *Br J Radiol*. 2006;79:248–253.
2. Saito T, Ohshima S, Xu WC. Size control of metal nanoparticle catalysts for the gas-phase synthesis of single-walled carbon nanotubes. *J Phys Chem B*. 2005;109:1064–1052.
3. Kelly KL, Coronado E, Zhao LL, et al. The optical properties of metal nanoparticles: The influence of size, shape, and dielectric environment. *J Phys Chem B*. 2003;107:668–677.
4. Phillip B, Garwin L. Science at the atomic scale. *Nature*. 1992;355:761–766.
5. Carvicchi RE, Silsbee RH. Coulomb suppression of tunnelling rate from small metal particles. *Phys Rev Lett*. 1984;52:1453–1456.
6. Yu L, Zhang Y. Preparation of nano-silver flake by chemical reduction method. *Rare Metal Materials and Engineering*. 2010;39:401–404.
7. Zhu HY, Orthman JA, Li JY, et al. Novel composites of TiO_2 (anatase) and silicate nanoparticles. *Chem Mater*. 2002;14:5037–5044.

8. Choy JH, Park JH, Yoon JB. Multilayered SiO_2/TiO_2 nanosol particles in two dimensional aluminosilicate catalyst-support. *J Phys Chem B*. 1998;102:5991–5995.
9. Mogyorosi K, Dékány I, Fendler JH. Preparation and characterization of clay mineral intercalated titanium dioxide nanoparticles. *Langmuir*. 2003;19:2938–2946.
10. Miao S. Liu Z, Han B, et al. Synthesis and characterization of TiO_2-montmorillonite nanocomposites and their application for removal of methylene blue. *J Mater Chem*. 2006;16:579–584.
11. Thomas JP. Intercalated clay catalysts. *Science*. 1983;220:365–371.
12. Morikawa Y. Catalysis by metal ions intercalated in layer lattice silicates. *Adv Catal*. 1993;39:303–327.
13. Thiripuranthagan S, Thangavelu K, Kannan S, et al. Noble metals intercalated/supported mica catalyst-synthesis and characterization. *J Mol Catal A Chem*. 2004;223:185–194.
14. Katz E, Willner I. Integrated nanoparticle-biomolecule hybrid systems: Synthesis, properties and applications. *Angew Chem Int Ed Engl*. 2004;43:6042–6108.
15. Sanchez C, Soler-Illia G, Ribot F, et al. Designed hybrid organic-inorganic nanocomposites from functional nanobuilding blocks. *Chem Mater*. 2001;13:3061–3083.
16. Haynes CL, van Duyne RP. Plasmon-sampled surface-enhanced Raman excitation spectroscopy. *J Phys Chem B*. 2003;107:7426–7433.
17. Tricokot YM, Fendler JH. Colloidal catalyst-coated semiconductors in surfactant vesicles: In situ generation of rhodium-coated cadmium sulfide particles in dihexadecyl phosphate vesicles and their utilization for photosensitized charge separation and hydrogen generation. *J Am Chem Soc*. 1984;106:7359–7366.
18. Dekany I, Turi L, Tombacz E, et al. Preparation of size-quantized CdS and ZnS particles in nanophase reactors provided by binary liquids adsorbed at layered silicates. *Langmuir*. 1995;11:2285–2292.
19. Papp S, Patakfalvi R, Dékány I. Metal nanoparticle formation on layer silicate lamellae. *Colloid Polym Sci*. 2008;286:3–14.
20. Ahmad MB, Shameli K, Darroudi M, et al. Synthesis and characterization of silver/clay nanocomposites by chemical reduction method. *Am J Appl Sci*. 2009;6:1909–1914.
21. Ahmad MB, Shameli K, Darroudi M, et al. Synthesis and characterization of silver/clay/chitosan bionanocomposites by UV-irradiation method. *Am J Appl Sci*. 2009;6:2030–2035.
22. Darroudi M, Ahmad MB, Shameli K, et al. Synthesis and characterization of UV-irradiated silver/montmorillonite nanocomposites. *Solid State Sci*. 2009;11:1621–1624.
23. Ahmad MB, Shameli K, Darroudi M, et al. Synthesis and antibacterial activity of silver/montmorillonite nanocomposites. *Res J Biol Sci*. 2009;4:1815–1846.
24. Ahmad MB, Shameli K, Darroudi M, et al. Antibacterial activity of silver/clay/chitosan bionanocomposites. *Res J Biol Sci*. 2009;4:1156–1161.
25. Goncharova SN, Paukshtisand EA, Balzhinimaev BS. Size effects in ethylene oxidation on silver catalysts. Influence of support and Cs promoter. *Applied Catal A: General*. 1995;126:67–84.
26. Sclafani A, Mozzanega M, Pichat P. Effects of silver deposits on the photocatalytic activity of titanium dioxide samples for the dehydrogenation or oxidation of 2-propanol. *J Photochem Photobiol A Chem*. 1991;59:181–189.
27. Hailstone RK. Computer simulation studies of silver cluster formation on AgBr microcrystals. *J Phys Chem*. 1995;99:4414–4428.
28. Nickel U, Castell AZ, Poppl K, et al. A silver colloid produced by reduction with hydrazine as support for highly sensitive surface-enhanced Raman spectroscopy. *Langmuir*. 2000;16:9087–9091.
29. Glaspell GP, Zuo C, Jagodzinski PW. Surface enhanced Raman spectroscopy using silver nanoparticles: The effects of particle size and halide ions on aggregation. *J Cluster Sci*. 2005;16:39–51.
30. Arroyo M, Lopez-Manchado MA, Avalos F. Crystallization kinetics of polypropylene: II Effect of the addition of short glass fibers. *Polymer*. 1997;38:5587–5593.
31. Velasco JI, Saja JA, Martınez AB. Crystallization behaviour of polypropylene filled with surface-modified talc. *J Appl Polym Sci*. 1996;61:125–132.
32. Hasmukh AP, Sumeet KS, Raksh VJ. Synthetic talc as a solid base catalyst for condensation of aldehydes and ketones. *J Mol Catal A Chem*. 2008;286:31–40.
33. Wesolowski M. Thermal decomposition of talc: A review. *Thermochim Acta*. 1984;78:395–421.
34. Aihara N, Torigoe K, Esumi K. Preparation and characterization of gold and silver nanoparticles in layered laponite suspensions. *Langmuir*. 1998;14:4945–4949.
35. Lin XZ, Teng X, Yang H. Direct synthesis of narrowly dispersed silver nanoparticles using a single-source precursor. *Langmuir*. 2003;19:10081–10085.
36. Liu FK, Hsu YC, Tsai MH, et al. Using γ-irradiation to synthesize Ag nanoparticles. *Mater Lett*. 2007;61:2402–2405.
37. Temgire MK, Joshi SS. Optical and structural studies of silver nanoparticles. *Radiat Phys Chem*. 2004;71:1039–1044.
38. Prasad V, Souza CD, Yadav D, et al. Spectroscopic characterization of zinc oxide nanorods synthesized by solid-state reaction. *Spectrochim Acta*. 2006;65:173–178.
39. Yang H, Du C, Jin S, Tang A. Preparation and characterization of SnO2 nanoparticles incorporated into talc porous materials (TPM). *Mater Lett*. 2007;61:3736–3739.